Molecular Catalysis 455 (2018) 68–77

Contents lists available at ScienceDirect

Molecular Catalysis

journal homepage: www.elsevier.com/locate/mcat

Study of the gas-phase glycerol oxidehydration on systems based on transition metals (Co, Fe, V) and aluminium phosphate

S. Lopez-Pedrajas[a,*], R. Estevez[a], J. Schnee[b], E.M. Gaigneaux[b], D. Luna[a], F.M. Bautista[a,*]

[a] Departamento Química Orgánica, Instituto Universitario de Investigación en Química Fina y Nanoquímica, Universidad de Córdoba, Campus de Excelencia Internacional Agroalimentario, CeiA3.Edificio Marie Curie, E-14014, Córdoba, Spain

[b] Institute of Condensed Matter and Nanosciences (IMCN) – MOlecules Solids and reactiviTy (MOST), Université Catholique de Louvain (UCL), Place Louis Pasteur 1, box L4.01.09, 1348, Louvain-la-Neuve, Belgium

ARTICLE INFO

Keywords:
Glycerol transformation
Acrylic acid formation
Supported cobalt oxide
Amorphous aluminium-cobalt phosphate
TPR
Propene oxidation

ABSTRACT

The gas-phase glycerol (Gly) transformation in the presence of oxygen has been studied on cobalt oxide systems (10 and 20 wt% Co) supported on a synthetic mesoporous aluminium phosphate ($AlPO_4$) calcined at 350 °C, as well as on a binary Co-Al phosphate with a Co content of 10 wt%. Synthetic binary phosphate of Al-M (M = Fe, V) have also been tested. The acidity (number and nature of acid sites) of the solids was determined by pyridine adsorption, whereas the reducibility was determined by H_2 TPR. The propene oxidation was employed as a test reaction. The influence of the amount of oxidant agent and the reaction temperature on both the glycerol conversion and the yield to reaction products was studied. The formation of acrylic acid; acetic acid and carbon dioxide was favoured for values of O_2/Gly ≥ 2 molar ratio and of temperatures beyond 250 °C. The Co oxide species in the supported systems that were the easiest to reduce (lower H_2 desorption temperature) exhibited the highest activity to produce acrylic acid. The formation of acetic acid and carbon dioxide was also promoted, suggesting the participation of the acid sites in addition to redox sites. Among the metals investigated here, Co would form part of the required catalyst for the formation of acrylic acid from glycerol. Based on the identified products in this study, some possible reactions involved in the glycerol transformation into oxidized compounds, have been suggested.

1. Introduction

The production of biodiesel generates glycerol as the main subproduct, which implies a financial and environmental problem in the biodiesel industry. The transformation of glycerol through several reactions has been widely studied giving rise to different valuable compounds such as hydrogen, acrolein (ACR), dihydroxyacetone, propylene glycol, glyceric acid, polyglycerol, glycerol ethers, glycerol ester, dioxolane and dioxane, etc [1,2]. Acrylic acid (AA) is one of these value-added chemical molecules, which has several uses such as adhesive, paint, plastics, superabsorbent polymer and rubber synthesis [3,4]. 85% of acrylic acid worldwide is produced from conventional acrolein usually on catalysts based on mixed oxides [5,6], traditionally starting from propene via two sequential oxidation steps [7]. Other alternatives to obtain acrylic acid are direct oxidation of propane [8,9] or sugar fermentation [10].

Obtaining acrylic acid from glycerol implies a two-step reaction, the first step being the dehydration of glycerol to acrolein, which has been widely studied on solid acid catalysts, as indicated in a recent review [11]. Given that acrolein is highly reactive, its storage and transport continue to be a challenge. Therefore, its transformation into a stable product by in-situ subsequent oxidation would solve these problems. The second step, the oxidation of acrolein into acrylic acid has not been the subject of extensive research, in contrast with glycerol dehydration.

The oxidehydration of glycerol to acrylic acid has been tested in both liquid [12–14] and gas phase [3,15–24], although the study has been developed much more in the latter. It is possible to carry out the reaction in the gas phase by using a single bifunctional catalyst via the one-pot approach [15–20,22,24] or by using a process that involves two separate steps with a double-catalyst bed [3,21,23]. One-step synthesis of acrylic acid from glycerol is more economically viable than the two-step transformation. Moreover, a potential advantage of bifunctional catalysts contained in a single catalytic bed would be the better long-term performance, although obtaining a bifunctional catalyst would be a more laborious task.

In the two-bed reactor approach, a high yield to acrolein (Y_{ACR}) is necessary in the dehydration step in order to avoid the oxidation of glycerol and to obtain a high yield to acrylic acid (Y_{AA}).

* Corresponding authors at: Departamento Química Orgánica, Universidad de Córdoba, Campus de Rabanales, Edificio Marie Curie, E-14014, Córdoba, Spain.
E-mail addresses: q52lopes@uco.es (S. Lopez-Pedrajas), fmbautista@uco.es (F.M. Bautista).

https://doi.org/10.1016/j.mcat.2018.05.020
Received 3 April 2018; Received in revised form 15 May 2018; Accepted 21 May 2018

Witsuthammakul et al. [3], by using HZSM-5 as the first catalytic bed and V-Mo oxides as the second, reported a Y_{AA} = 38%, while the mixture of both catalysts promoted the direct oxidation of glycerol to an undesirable oxygenated C_2, therefore producing less amount of acrylic acid. The same conclusion was achieved by Liu et al. [21] who reported a Y_{AA} = 75% by using $Cs_{2.5}H_{0.5}PW_{12}O_{40}$ supported on Nb_2O_5 and vanadium-molybdenum oxides supported on the silicon carbide. This high Y_{AA} was obtained given that the optimum reaction temperature and the oxygen/glycerol ratio for these two catalysts were very similar.

For the one-step method, Deleplanque et al. [15] at 280 °C obtained a Y_{AA} = 28% on MoVTeNbO, but also a yield to acetic acid of 23% and to CO_x of 45%. Wang et al. [16] reported a Y_{AA} = 14% at 300 °C with iron oxide embedded in an iron orthovanadate, acrolein (28%) and acetic acid (24%) being the main products. They emphasize that the distance between the two phases of the solid was very important in its catalytic performance. Possato et al. [22] reported a Y_{AA} = 16% on V_2O_5/MF1, the importance of vanadium oxide species standing out in the conversion of acrolein to acrylic acid and in the oxidation of coke formed from glycerol. Nieto et al. [17,18,20] achieved a Y_{AA} = 50.5% at 265 °C on W-V-Nb mixed oxides with a hexagonal tungsten bronze structure, with productivity values of industrial relevance. They have also reported [24] that the formation of acrylic acid requires a close proximity of both acid and redox sites as well as acid sites with a sufficient strength to catalyse the dehydration reaction, allowing the desorption of acrylic acid.

We have previously studied the glycerol dehydration in the absence of oxygen over catalysts based on an amorphous mesoporous aluminium phosphate ($AlPO_4$) in liquid [25] and gas [26,27] phases, obtaining better results in the gas phase. The modification of aluminium phosphate with small amounts of a transition metal, especially V (~3 wt%) [26], as well as Fe and Co (1 wt%) [27], gave rise to more active and selective catalysts to produce acrolein. Hence, the activity of the phosphates depends not only on their acidity (mainly acid sites of weak-medium strength), but also on the redox sites. Furthermore, the phosphates showed a high stability, not undergoing deactivation after 22 h of reaction [27]. Taking these previous results into account, in the present paper we studied the capacity of Al-M phosphates with a higher amount (10 wt%–37 wt%) of Co, Fe and V to catalyse the transformation of glycerol to acrylic acid, via acrolein formation, in the presence of oxygen. In addition to those Al-M binary phosphates, we have also synthesized new systems of Co supported on $AlPO_4$. The structural characterization of the solids was carried out by X-ray diffraction (XRD) and ^{27}Al and ^{31}P Magic Angle Spinning Nuclear Magnetic Resonance (MAS NMR) spectroscopy. Likewise, their textural properties were determined, as well as the surface acidity and the nature of the acid sites through pyridine (Py) chemisorption, by Temperature Programmed Desorption (TPD) and Diffuse Reflectance Infrared Fourier Transform (DRIFT), respectively. CO_2 chemisorption was employed to evaluate the basic properties of the solids, whereas H_2 Temperature Programmed Reduction (TPR) was used to evaluate the capacity of reducibility. Moreover, the propene oxidation was also employed in evaluating the redox sites.

2. Experimental

2.1. Catalyst preparation

The Co systems (10 and 20 wt%) were obtained by impregnation of a synthetic amorphous aluminium phosphate, $AlPO_4$, calcined at 350 °C (molar ratio P/Al = 1; S_{BET} = 248 m^2/g; dp = 182 Å) with a solution of $Co(NO_3)_2{\cdot}6H_2O$ in methanol. After drying, the solids were calcined in air for 3 h at 450 °C. These solids will be denoted as $xCo/AlPO_4$-T, where x represents the percentage in weight of Co and T, the calcination temperature.

The Al-Co phosphate (P/(Al + Co) = 1; Al/Co = 3.5; 10 wt% of Co) was prepared by a sol-gel method as previously reported [27], from aqueous solutions of $AlCl_3{\cdot}6H_2O$ and $Co(NO_3)_2{\cdot}6H_2O$ and H_3PO_4 (85 wt %). The precipitation agent, aqueous ammonia (25 wt%), was slowly added stirring at 0 °C. The pH value at the precipitation 'end point' was 6.7. After filtration, the solid was washed with 2-propanol and dried at 120 °C for 24 h.

For the synthesis of Al-Fe and Al-V phosphates, an aqueous solution of $Fe(NO_3)_3{\cdot}9H_2O$ and vanadyl oxalate, respectively, were employed as previously reported [28,29]. The amount of Fe in the Al-Fe phosphate was 20.5 wt% (molar ratio Al/Fe = 1) [28], whereas the amount of V in the Al-V phosphates was 27 wt% (Al/V = 0.6) and 37 wt% (Al/V = 0.2) [29].

The binary phosphates will be denoted as AlMPO(x)T, where x indicates the Al/M theoretical molar ratio and T, the calcination temperature.

As a reference, simple phosphates of Al ($AlPO_4$); Co ($Co_3(PO_4)_2$) and Fe ($FePO_4$) were also synthesized by the aforementioned method with a molar ratio P/M = 1 [26,27].

All the solids were calcined at 450 °C in air for 3 h, and screened at < 0.149 mm to avoid internal diffusion limitations in the reaction.

2.2. Characterization of catalysts

The textural properties were determined from the adsorption–desorption isotherms of nitrogen at its liquid temperature (–196 °C), using a Micromeritics ASAP 2000 apparatus. Prior to measurements, all samples were degassed to 0.1 Pa. BET surface areas were determined applying equation at relative pressures in the range p/p_0 = 0.05-0.30, assuming a cross-sectional area of 0.162 nm^2 for the nitrogen molecule. The pore size distribution was calculated using the method of Barrett, Joyner and Halenda (BJH) assuming a cylindrical pore model.

X-ray diffraction (XRD) patterns were obtained using Ni-filtered Cu K_α radiation (λ = 1.5418 Å). Finely ground samples were scanned at a speed of 2°/min (2θ = 2–80°) using a Siemens D-500 diffractometer (40 kV, 30 mA).

^{31}P and ^{27}Al nuclear magnetic resonance spectra were collected on a BRUKER AVANCE 400WB spectrometer using a 4 mm BRUKER double resonance MAS probe. All experiments were performed at room temperature. ^{27}Al and ^{31}P MAS NMR were recorded at resonance frequencies, υ_0, of 104.26 MHz and 161.98 MHz, respectively. $Al(H_2O)_6^{3+}$ and H_3PO_4 solutions were used as external standard references for Al and P chemical shifts, respectively. The data were processed by Fourier transformation, phase correction and baseline correction using the Dm2005test NMR data processing software.

Total acidity was measured by Temperature Programmed Desorption of pyridine (Py-TPD), using an apparatus from PID Eng& Tech with a TCD (thermal conductivity detector). Before the adsorption experiments started, the catalyst (30 mg) was pre-treated in situ from room temperature to 400 °C (rate of 20 °C/min). After the catalyst pretreatment, saturation of the sample with pyridine was carried out at 50 °C for 30 min, thereafter, physisorbed pyridine was desorbed at 50 °C for 60 min. Then the measurements were performed in the range of 50–450 °C, with a heating rate of 10 °C/min to remove the chemisorbed pyridine.

Diffuse Reflectance Infrared Fourier Transform (DRIFT) spectra of adsorbed Pyridine were recorded on a FTIR instrument (Bomem MB-3000) equipped with an "environmental chamber" (Spectra Tech) placed in a diffuse reflectance attachment (Spectra Tech, Collector). A resolution of 8 cm^{-1} was used with 256 scans to obtain a spectrum from 4000 to 600 cm^{-1}. The reference spectrum of the sample was recorded at 350 °C. Pyridine (99.8% from Aldrich) adsorption was carried out at 120 °C for a certain period of time (typically 1 h), allowing the saturation of the catalyst surface. The samples were subsequently degassed in 4 stages of 1 h each at 50 °C, 150 °C, 200 °C and 300 °C, respectively.

H_2 TPR experiments were performed on a Micromeritics Autochem

Table 1
Textural properties and acidity measurements from Py-TPD and B/(L + B) ratio for each catalyst after pyridine degassing for 1 h at 150 °C and 300 °C.

Catalyst	S_{BET} (m^2/g)	V_P (mL/g)	d_P (Å)	Pore size distribution (%)			Acidity		Strength of acid sites (%)			Acid sites nature	
				> 500 Å	500 − 20 Å	< 20 Å	(μmol/g)	(μmol/m^2)	Weak (80–200 °C)	Medium (200–300 °C)	Strong (> 300 °C)	B/(L + B) (150 °C)	B/(L + B) (300 °C)
10Co/$AlPO_4$-450	152.9 ± 0.5	0.64	166	14	86	–	143	0.9	59	22	19	0.11	0.07
20Co/$AlPO_4$-450	132.1 ± 0.4	0.52	158	17	83	–	128	1.0	57	20	22	0.22	0.34
AlCoPO(3.5)450	129.3 ± 0.4	0.71	220	23	77	–	106	0.8	63	22	15	0.32	0.36
$AlPO_4$450	199.1 ± 0.8	0.82	165	12	87	–	144	0.7	72	20	8	0.47	0.38
$Co_3(PO_4)_2$450	8.2 ± 0.1	0.06	290	57	43	–	4	0.5	–	–	–	–	–
AlFePO(1)450	97.2 ± 0.2	0.29	120	–	89	11	119	1.2	77	12	11	0.18	0.23
$FePO_4$450	55.8 ± 0.1	0.31	223	25	75	–	150	2.7	63	25	12	0.25	0.61
AlVPO(0.6)450	7.84 ± 0.03	0.02	103	99	1	–	13	1.7	51	27	22	0.65	–
AlVPO(0.2)450	1.91 ± 0.08	0.01	243	–	–	–	3	1.6	–	–	–	–	–

2910 analyser. Samples of 50 mg were first treated in Ar at 150 °C for 1 h and then put into contact with an H_2/Ar mixture (10 mol% of H_2; 50 mL/min) and heated (5 °C/min) to a final temperature of 950 °C. The amount of H_2 consumption was estimated from the peak area in the TPR profiles.

The basicity of the samples was evaluated by CO_2-chemisorption on a Micromeritics ASAP2010 Chemi apparatus. The U-shaped sample tube containing 150 mg of the catalysts was first flushed under a He (Praxair, 99.9997%) flow at 300 °C for 2 h and then evacuated for 2 h down to a residual pressure ($< 6.6{\cdot}10^{-7}$ MPa). A first CO_2 (Praxair, 99.2%) adsorption isotherm was recorded at 50 °C. Then the sample was evacuated at the same temperature and a second CO_2 adsorption isotherm was measured. From the difference between the two isotherms, the amount of carbon dioxide chemisorbed on the sample at 50 °C, was obtained. The interception of a linear interpolation done on the difference points measured between 0.026 and 0.091 MPa, was taken as a measure of the total basicity of the samples.

The oxidation of propene was carried out in a continuous flow fixed bed reactor under atmospheric pressure in a U-shaped quartz reactor. The catalyst particles (150 mg; 200 μm < Ø < 315 μm) were mixed with quartz spheres (100 μm < Ø < 315 μm) until the catalytic bed reached 1 mL. The temperature was monitored by a thermocouple located in the catalyst bed. The reaction mixture was analysed using an on-line Varian GC CP3800 equipped with three detectors. A Hayesep column coupled with a Molecular Sieve column and a thermal conductivity detector (TCD), were used to separate and quantify O_2, N_2, CO, CO_2, C_3H_6 and C_3H_4O. Likewise, C_3H_6, C_3H_4O and other compounds were analysed in a DB-5MS column ((5%-Phenyl)-methylpolysiloxane, 50 m × 0.25 mm × 25 μm) coupled with a flame ionization detector (FID). A blank test showed the absence of homogeneous reactions, as well as the inactivity of the quartz spheres and the reactor.

2.3. Catalytic test

The glycerol transformation was carried out in a continuous-flow fixed bed reactor (9 mm internal diameter and 230 mm long) under atmospheric pressure. The temperature was monitored by a thermocouple located in the catalyst bed. The reaction mixture was collected in two consecutive ice traps, which were then analysed without preliminary extraction or separation of water. The analysis was carried out by gas chromatography (GC) equipped with a FID using a Supelcowax-10 column (100% poly(ethylene glycol), 30 m × 0.25 mm × 25 μm). In addition, a molecular sieve was used to quantify the CO_2 production, measuring the volume of CO_2 formed during the reaction. The formation of CO was discarded by using a TCD.

The catalyst (0.2 g, < 0.149 mm) was mixed with silicon carbide (0.325–0.425 mm) until 0.6 g. The mixture was pre-treated at the reaction temperature for 2 h in a N_2 flow (75 mL/min). A 36 wt% glycerol (99.5%, Sigma-Aldrich) aqueous solution was fed at 0.6 mL/h ($2.54 \cdot 10^{-3}$ mol/h of glycerol), which resulted in a contact time of 4.72 g_{cat}·min/mmol. The products were identified through chromatographic patterns and/or GC–MS as previously reported [27]. A blank test showed the absence of homogeneous reactions and the inactivity of the reactor and the silicon carbide.

In order to avoid the polymerization of acrolein, hydroquinone was added (0.3 wt%) to the aqueous solution of glycerol in the feed and also to the cold traps where the reaction products were collected. The hydroquinone also allowed the carbon balance to be estimated.

The glycerol conversion (X_{Gly}) was calculated from $X_{Gly} = (mol_{Gly,in}\text{-}mol_{Gly,out})\cdot 100/mol_{Gly,in}$, whereas the selectivity (Si) and the yield (Yi) to product i were expressed as mol% on a C atom basis.

The rate values of the product formation (r_i) were obtained from the yield values by the equation $r_i = Y_i \cdot F_{Gly}/100 \cdot w$, where w is the catalyst weight (g) and F_{Gly} is the feed rate of glycerol (μmol/s).

Carbon balance (mol%) was calculated by summing up the amount of unreacted glycerol and the total quantities of the identified products.

3. Results and discussion

3.1. Characterization of the solids

3.1.1. Textural properties

Concerning the textural analysis, the nitrogen isotherms obtained for all the solids studied were type IV of the Brunauer, Deming and Teller (BDDT) classification, exhibiting a H1 hysteresis loop that indicates the presence of mesoporous solids. Furthermore, t-plots (using Harkins-Jura correlation) from the adsorption branch of the isotherm showed the absence of microporosity, with the exception of the Al-Fe phosphate, Table 1. However, the solids with V presented a reversible type II nitrogen isotherm without hysteresis, characteristic of the non-porous adsorbents [29]. The values of surface area, S_{BET}, pore volume, V_p, and of mean pore diameter, d_p, as well as the pore size distribution obtained for the solids, are compiled in Table 1. It can be seen that among the simple phosphates, the $AlPO_4$450 showed the highest surface area (S_{BET} = 199.1 m^2/g) and pore volume (V_p = 0.82 mL/g) and the smallest pore diameter (d_p = 165 Å). With the addition of any metal, the $S_{BET,}$ as well as the $V_{P,}$ decreased in respect to the $AlPO_4$450. In the 10Co/$AlPO_4$-450 the S_{BET} decreased by 23%, whereas the decrease was 35% in the coprecipitated solid, this loss being almost the same as in the 20Co/$AlPO_4$-450 (34%). It was also remarkable that the d_P increased in the AlCoPO(3.5)450, while in the supported systems, it remained practically constant. Furthermore, with the exception of the simple Co phosphate that exhibited a slightly higher percentage of macropores (> 500 Å) than mesopores (500–20 Å), in the rest of the porous solids the mesopores predominated. Regarding the solids with V, they exhibited very low S_{BET} values, given their non-porous character.

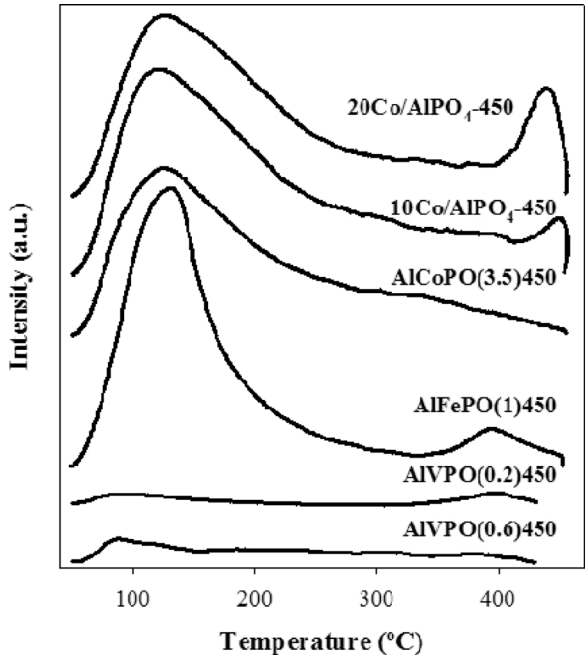

Fig. 1. Pyridine-TPD profiles for some of the solids studied.

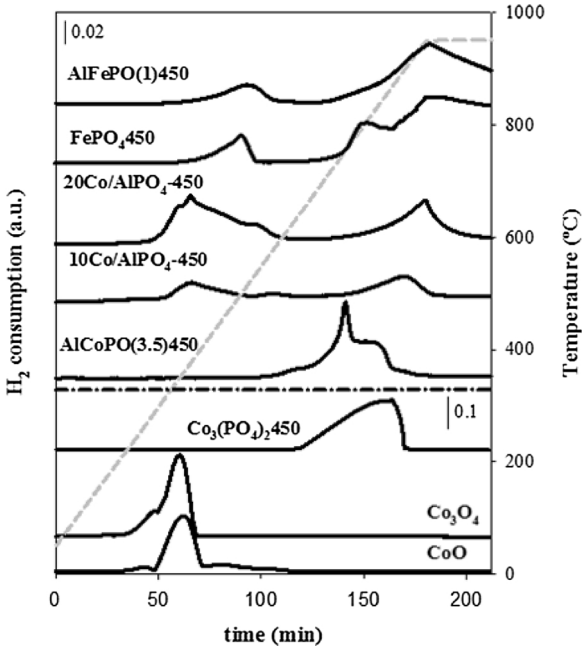

Fig. 2. TPR profiles for some of the solids studied.

3.1.2. Acid and base properties

Regarding the results from the Py-TPD, the systems containing cobalt and iron exhibited a similar profile, Fig. 1, to that previously obtained for $AlPO_4$ [26], with a maximum intensity between 100 °C and 200 °C. In addition, a second maximum between 400 °C and 450 °C was observed for 10Co/$AlPO_4$-450 and 20Co/$AlPO_4$-450, and at 395 °C for AlFePO(1)450. For the systems containing vanadium, the desorbed pyridine was practically negligible, as indicated by the almost flat profiles obtained.

Table 1 shows the total acidity of the solids and the distribution of the acid sites according to their strengths following the criteria indicated. Normally, the higher the S_{BET}, the higher the acidity value. Thus, the $AlPO_4$450 was the simple phosphate with the highest acidity (144 μmol/g). With the addition of a 10 wt% of Co, the total acidity decreased by 26% in the coprecipitated solid, remaining practically unchanged in the impregnated system, whereas both solids experimented an increment in the percentage of strong acid sites, which was more noticeable in the impregnated solid. With the addition of a 20 wt % of Co, the acidity and the strength followed the same tendency, while the density of acid sites increased with the percentage of Co. In the AlFePO(1)450, a decrease in the total acidity (but an increase in the density) was observed, as well as a decrease in the medium acid sites.

The DRIFT spectroscopy distinguishes between Lewis (L) and Brönsted (B) acid sites. In order to estimate which ones were more abundant and their respective strengths, the B/(L + B) ratio has been calculated at two temperatures 150 °C and 300 °C of desorbed pyridine, Table 1. As can be seen, all the phosphates possessed both kinds of acid sites, the $AlPO_4$ showing a majority of Lewis. The formation of Lewis acid sites was favoured by the addition of a second metal, with the exception of V. For the same amount of Co, the impregnated solid had more Lewis acid sites than the coprecipitated system, whereas in the 20Co/$AlPO_4$-450, the Lewis acid sites decreased with respect to the 10Co/$AlPO_4$-450. The high percentage (61%) of the strong Brönsted acid sites in the $FePO_4$ is remarkable, although the modification of $AlPO_4$ with Fe produced a decrease in the Brönsted acid sites.

In the CO_2-chemisorption experiments, under the present experimental conditions, chemisorption of CO_2 was not observed with any of the solids studied. This could be due to the amount of desorbed CO_2 being inferior to that required by the sensitivity of the instrument. However, Bautista et al. [30] previously published that a $AlPO_4$ synthetized by the same method and calcined at the same temperature, adsorbed 92 μmol/g of CO_2 in a TPD experiment. Likewise, the titration of $AlPO_4$ with a cyclohexane solution of benzoic acid gave a positive result [31]. Consequently, the presence of basic sites in the solids studied here should not be ruled out.

3.1.3. Reducibility

As far as the TPR profiles of the solids are concerned, they are presented by the H_2 consumption as a function of the temperature in Fig. 2, and the corresponding values of consumption of H_2 per g of catalyst and per at-g of metal, are collected in Table 2. For the calculation of the values per at-g of metal, the theoretical metal content in the catalysts containing Co was used, whereas the Fe and V content was that obtained by ICP analysis, as previously reported [28,29].

Table 2
H_2 consumption and temperature of each peak after deconvolution from TPR of all the solids studied.

Catalysts	Temperature (°C)	H_2 (mmol/g)	H_2/at-g_M ($mmol_{H2}$/mat-g_M)
10Co/$AlPO_4$-450	380	1.3	0.8
	580	0.3	0.2
	900	1.7	1.0
20Co/$AlPO_4$-450	378	3.0	0.9
	532	0.8	0.2
	949	2.4	0.7
AlCoPO(3.5)450	665	0.7	0.4
	752	1.8	1.1
	807	1.5	0.9
$Co_3(PO_4)_2$450	863	25.3	3.1
CoO	363	8.8	0.7
Co_3O_4	290	3.5	0.3
	353	10.4	0.8
AlFePO(1)450	512	1.2	0.4
	830	1.3	0.4
	950	6.3	1.9
$FePO_4$450	506	1.5	0.3
	810	2.5	0.4
	950	13.2	2.4
AlVPO(0.6)450	508	2.0	0.5
AlVPO(0.2)450	505	3.0	0.5

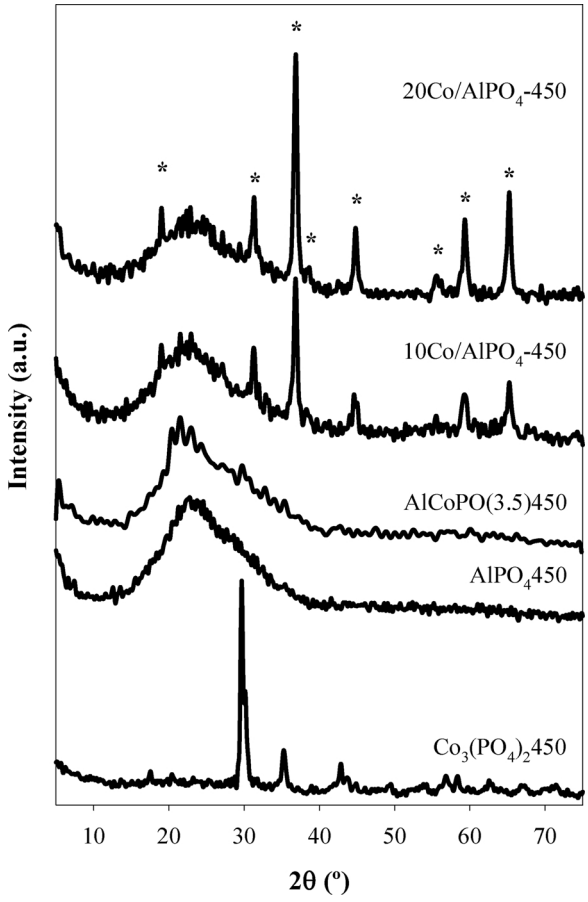

Fig. 3. XRD patterns for some of the solids studied (*Co_2AlO_4).

As can be seen in Fig. 2, the profiles of both Co supported systems were similar with maxima in the 380–580 °C temperature range and another peak around 900 °C. The maximum around 380 °C can be assigned to Co oxide species according to the profiles obtained by two commercial Co oxides. Thus, the Co_3O_4 reduction to metallic cobalt would take place in two consecutive steps: $Co_3O_4 \rightarrow CoO \rightarrow Co$ at 290 °C and around 350 °C, respectively [32]. The H_2/M values (around 1) for these solids, Table 2, is in accordance with this assignation. The small peak at 580 °C could indicate an interaction of Co oxide species with the support [32]. In fact, the peak at 900 °C could be assigned to Co_2AlO_4 according to the literature [33,34]. Furthermore, the profile of the AlCoPO(3.5)450 started at 600 °C indicating Co species, which are more difficult to reduce than those of Co oxides. However, the Al presence in the Co phosphate promoted the reduction of the Co species according to the difference in the profiles of the binary and simple Co phosphates. The asymmetric profiles exhibited by both phosphates, as well as the high value of the H_2/Co ratio, were in agreement with the existence of Co^{2+} species with different coordinations and of Co^{+3} species [27], although the main phase of Co phosphate was a $Co_2P_2O_7$ (JCPDS 34–1378) [26], Fig. 3.

The profiles of the reduction of $FePO_4$450 and AlFePO(1)450, Fig. 2, showed three asymmetric reduction peaks at 506, 810 y 950 °C, that can be assigned to the following reactions: $FePO_4 \rightarrow Fe_3(P_2O_7)_2 \rightarrow Fe_2P_2O_7 \rightarrow Fe$ [35,36]. However, the first reduction peak of the AlFePO(1)450 started at a lower temperature than that of $FePO_4$450, indicating once again the favourable effect of Al in the reduction of Fe species [37]. The TPR profiles of the Al-V phosphates [38] revealed the existence of various types of vanadium species, β-$VOPO_4$ and V_2O_5, in each catalyst, whose reduction took place in two temperature intervals, 290 °C–698 °C ($V^{+5} \rightarrow V^{+4}$) and 773 °C–950 °C ($V^{+4} \rightarrow V^{+3}$).

3.1.4. Structural characterization

The XRD analysis of the Co supported systems corroborated the formation of a Co_2AlO_4 spinel (JCPDS 38-0814), Fig. 3. Furthermore, the amorphous character of $AlPO_4$450 is retained in both supported systems and in the AlCo binary phosphate. On the contrary, the simple Co phosphate exhibited a crystalline character which is in accordance with the textural properties exhibited.

Likewise, the ^{31}P and ^{27}Al MAS NMR spectra also indicated the interaction of the Co species with the $AlPO_4$. Thus, all the ^{31}P MAS NMR spectra, Fig. 4, showed a peak around −25 ppm typical of tetrahedrally coordinated phosphorous in amorphous aluminium phosphates [27,39]. In the AlCoPO(3.5)450 spectrum in particular, this signal was wider and shifted toward the upper field, probably due to the presence of Co in the second coordination sphere of phosphorous, $P(OAl)_3(OCo)$. In fact, after the deconvolution of the signals, a new component around −13 ppm appeared, which was especially important in the coprecipitated system. However, the ^{27}Al MAS NMR results indicated significant differences between the coprecipitated and supported solids, Fig. 4. Thus, the spectrum of the coprecipitated system was similar to that of $AlPO_4$, with a signal around 38 ppm corresponding to $Al(OP)_4$ [27]. In

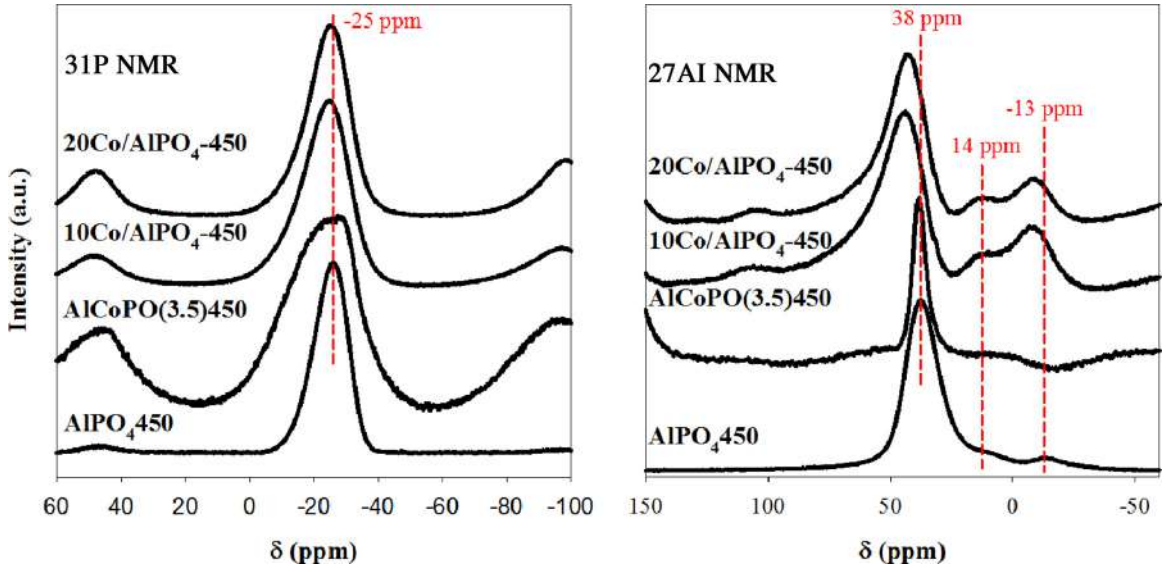

Fig. 4. ^{31}P and ^{27}Al MAS NMR spectra for some of the solids studied.

Table 3
Propene conversion (X_{C3H6}) and rate of production of different products at steady state (T = 400 °C; w = 0.15 g; F_{C3H6} = 2.15 mL/min; F_{air} = 5.35 mL/min; F_{He} = 7.5 mL/min; time on stream = 3 h).

Catalysts	X_{C3H6} (mol %)	r_{ACR}	r_{CO2}	r_{CO}	$\frac{\mu mol_{ACR}}{mat-g_M \cdot min}$	$\frac{\mu mol_{CO_2}}{mat-g_M \cdot min}$
		$\mu mol/g_{cat} \cdot min$				
10Co/$AlPO_4$-450	8	1.1	40.8	2.3	0.6	24
20Co/$AlPO_4$-450	12	0.6	71.9	0.9	0.2	21
AlCoPO(3.5)450	4	1.9	11.0	1.8	1.1	6
$AlPO_4$450	5	1.5	15.6	2.6	–	–
$Co_3(PO_4)_2$	3	1.4	8.1	1.1	0.2	1
$FePO_4$450	5	2.7	15.1	2.2	0.4	2
AlVPO(0.6)450	15	3.8	26.8	11.6	0.9	6

the impregnated solids, this signal was wider and shifted towards the lower field, indicating the formation of the spinel Co_2AlO_4. Likewise, the peaks around 14 and −13 ppm, that increased in relation to those in the $AlPO_4$450 spectrum, could be assigned to the octahedral coordination $Al(OP)_4(H_2O)_2$ and to the pentahedral coordination [27,39], respectively.

3.1.5. Propene oxidation

The reaction of propene oxidation was carried out under the following experimental conditions: 400 °C, 0.15 g of catalyst, 2.15 mL/min of propene, 5.35 mL/min of air and 7.5 mL/min of helium, in which the absence of diffusional problems was confirmed. Under these kinetic conditions, the main products detected were acrolein and products of total oxidation, mainly CO_2. The formation of undetected products and/or of polymeric products cannot be ruled out, taking into account the mismatch of the C balance during the reaction, especially at the beginning. In fact, in all the catalysts after 15 h of reaction, the formation of coke was verified, obtaining approximately 15 wt%, according to the thermogravimetric analysis.

Table 3 shows the propene conversion and the formation rate of acrolein, CO_2 and CO values obtained on all the catalysts at the steady state (3 h of time on stream). At the beginning of the reaction, the selectivity to acrolein decreased while the selectivity to CO_2 increased. Hence, the formation of carbon oxides probably took place from the direct oxidation of propene and/or acrolein, as well as from the gradual combustion of coke products formed over the catalysts. As can be seen, on all the catalysts, the formation of carbon oxides predominated with respect to the acrolein formation. This fact was more evident in the supported systems, the 20Co/$AlPO_4$-450 exhibiting the highest formation rate of carbon oxides (72 ± 1 $\mu mol/g_{cat} \cdot min$). The activity to produce acrolein and carbon oxides of $AlPO_4$ is noticeable, taking into consideration that it does not possess redox properties. Therefore, the formation of acrolein (and subsequent oxidation) from propene cannot only be explained by a Mars-van Krevelen mechanism [40].

3.2. Glycerol transformation in the presence of oxygen

Under the current experimental conditions, acrylic acid (AA), acetaldehyde (ACE), acetic acid (AcA) and CO_2, were detected. In addition, the typical compounds obtained in the absence of oxygen, acrolein (ACR) and hydroxyacetone (HA), and the product of glycerol acetalization with formaldehyde, glycerol formal (GF), were also detected. The formation of ACE is remarkable given that in the absence of oxygen, it had never been detected previously [26,27], in spite of being a widely reported reaction product in the glycerol dehydration [11]. Methylglyoxal (MG) was also detected. Regarding the "Unknown" compounds, they include those compounds detected only in traces (ethanol, formic acid, formaldehyde, oxalic acid and glycidol), those detected but not identified, as well as non-detected compounds, which could be implied in the coke formation [26,27]. The yield values to these "Unknown" compounds have been calculated subtracting the sum of the yields to detected products from the conversion. Some other products were quantified but in smaller amounts, as 2-ethyl-4-methanol-1,3-dioxalane, 1,3-propanedioldiacetate and phenol.

3.2.1. Influence of the reaction parameters

The influence of the amount of oxidant agent and the reaction temperature on the conversion (X_{Gly}) and yield to reaction products was studied, in order to determine the optimal conditions of reaction. In the study of each parameter, a single load of catalyst was employed. However, before changing one variable, the glycerol flow was stopped and the catalyst was treated with O_2 and N_2. In Figs. 5 and 6 the results obtained on AlVPO(0.6)450 at 3 h of reaction are shown.

The change of conversion and yield values as a function of the molar ratio O_2/Gly, by varying the F_{O2} and maintaining the F_{Gly} constant, is shown in Fig. 5. As can be seen, the X_{Gly} increased gradually with the increase of the flow of O_2, in accordance with that reported by Wang and Chieregato [16,20], which revealed the importance of O_2 in the reaction. Likewise, adding O_2 as a reagent produced a decrease in the yield to dehydration products, acrolein and hydroxyacetone, as was reported by Wang et al. [16], as well as in the yield to the "Unknown" compounds. Methylglyoxal was detected both in the presence and in the

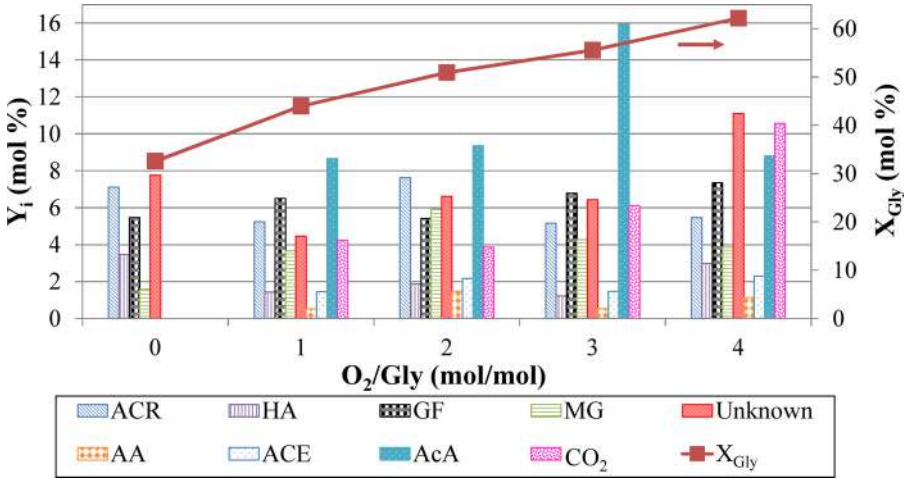

Fig. 5. Glycerol conversion (X_{Gly}) and yield to reaction products (Y_i) values on AlVPO(0.6)450 as a function of molar ratio O_2/Gly. Reaction conditions: 36 wt% glycerol; F_{Gly} = 0.7 μmol/s; F_{N2} = 17 mL/min; w = 0.2 g; 280 °C; time on stream = 3 h with O_2 and 1 h without O_2.

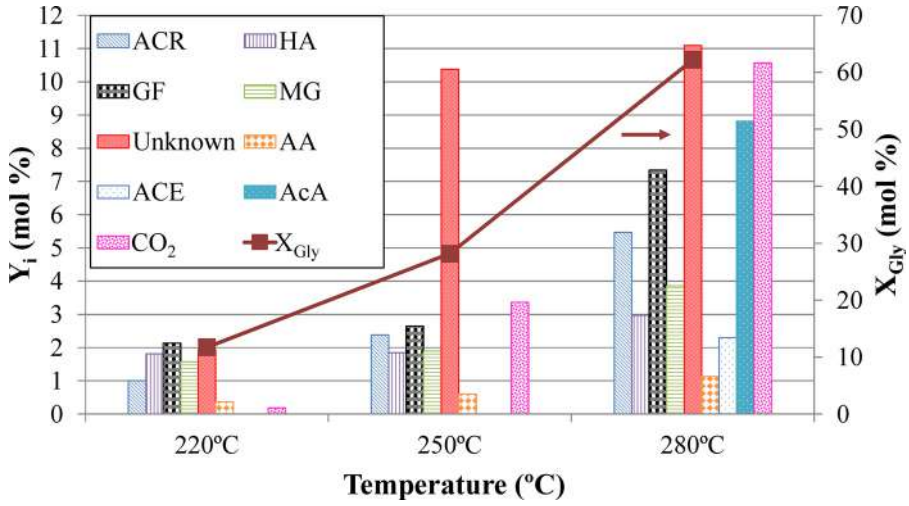

Fig. 6. Glycerol conversion (X_{Gly}) and yield to reaction products (Y_i) values on AlVPO(0.6)450 as a function of reaction temperature. Reaction conditions: 36 wt% glycerol; F_{Gly} = 0.7 μmol/s; F_{N2} = 17 mL/min; F_{O2} = 4 mL/min; w = 0.2 g; 280 °C; time on stream = 3 h.

absence of O_2, although the yield values were greater in the presence of O_2 as expected, given that the oxidative dehydrogenation is favoured [3] with respect to the reaction in the absence of oxygen, due to its endothermic and reversible character. However, in the absence of O_2 it was also formed, as happened in the 2-propanol transformation in which the formation of propanone on this same catalyst took took place [29]. The yield to methylglyoxal attained a maximum for O_2/Gly = 2, and slightly decreased for superior values. An increase in the methylglyoxal yield implied a decrease in the yield to hydroxyacetone, hence its formation could take place most probably by dehydrogenation of hydroxyacetone. Regarding the formation of glycerol formal, the yield values remained practically unchanged with the molar ratio O_2/Gly.

The highest selectivity and yield to acrylic acid was also obtained for values of O_2/Gly molar ratio = 2, in accordance with some reported studies [15,17,18,20]. A higher flow of O_2 could give rise to the total oxidation of AA. In fact, at O_2/Gly ≥ 2 the formation of "Unknown" compounds and acetic acid, as well as of the total oxidation product, CO_2, was promoted. The acrolein and/or hydroxyacetone (or methylglyoxal) could also contribute to the formation of these compounds, given that their yield values decreased as the oxygen was in excess. In this respect, Liu et al. [23] reported 3-hydroxypropionaldehyde and hydroxyacetone as the main sources of CO_x formation. Likewise, Soriano et al. [17] reported that the secondary reactions of acrolein gave rise to CO_x.

In regard to the influence of the reaction temperature, Fig. 6, the glycerol conversion increased with the temperature as expected, according to the results reported [17,19,20,22]. However, this increase of conversion, especially above 250 °C, implied the formation preferably of CO_2, acetic acid and "Unknown" compounds, although the formation of these last compounds greatly increased between 220 °C and 250 °C. The increase of yield to acrolein and hydroxyacetone (or MG) was less pronounced in the temperature range studied. The same tendency was observed in the case of acrylic acid, whose maximum yield value was around 1% at 280 °C. As can also be seen in Fig. 6, the formation of acetaldehyde and acetic acid needs the highest temperature studied, 280 °C. In the presence of oxygen, an increase of yield to acrolein was reported within the range of 300 °C–320 °C, although at higher temperatures a decrease of yield took place [19,22].

Based on the identified products in the present study, the reactions involved in the glycerol transformation, which we previously reported [26], could be extended as shown in Scheme 1. Thus, acetaldehyde, formed from 3-hydroxypropanaldehyde by a retro aldol condensation, is oxidized to acetic acid, which could react with 1,3 propanediol (a reduction product of 3-hydroxypropanaldehyde) giving rise to 1,3-propanedioldiacetate. The acrolein can undergo an oxidation to acrylic acid or a reduction to propanaldehyde, which could react with glycerol producing 2-ethyl-4-methanol-1,3-dioxolane. Many routes generating CO_2 are suggested in Scheme 1.

3.2.2. Catalytic behaviour of the solids

Fig. 7 shows the values of glycerol conversion and of acrylic acid formation rate obtained over the solids studied. As can be seen, the highest values of conversion (around 90%) were obtained for the solids containing Fe, followed by those with Co (around 75%), and finally by those with V (around 50%). However, the most active solids in the acrylic acid formation were the two Co supported systems, which exhibited a similar yield (~2%) and rate (4.1 μmol/g_{cat}·min) values. It is remarkable that for the same percentage of Co (10 wt%), the supported system, 10Co/$AlPO_4$-450, was more active in the glycerol transformation and, specifically in the acrylic acid formation, than that obtained by precipitation, AlCoPO(3.5)450. Furthermore, the presence of Al in the Fe and V phosphates promoted the formation of acrylic acid. Thus, the Al-Fe phosphate was more active than the $FePO_4$, and the AlVPO (0.6)450 (with a greater amount of Al) being more active than AlVPO (0.2)450. The lower activity of this binary phosphate could be related to the presence of V_2O_5 in addition to the main phase of β-$VOPO_4$ [29]. In fact, Shen et al. [19] reported the inactivity of V_2O_5 for producing acrylic acid in the temperature range of 250–350 °C, whereas Possato et al. [22] reported a very low activity, X_{Gly} (40%) and Y_{AA} (2%), at 350 °C.

In an experiment carried out on a double catalytic-bed [0.1 g $AlPO_4$450 + 0.1 g $Co_3(PO_4)_2$450], both X_{Gly} and r_{AA} increased in relation to the values obtained for the binary phosphate, Fig. 7. However, the Co content in the double bed was the highest (24 wt%). In fact, as shown in Fig. 8, the Al-Co phosphate exhibited a slightly higher activity in the AA formation per at-g of Co than that reached on the double catalytic-bed. As can also be seen in Fig. 8, the Co was the most effective metal producing AA, the systems prepared by impregnation standing out, especially the system with the lowest content, 10Co/$AlPO_4$-450. Once again, the positive effect of Al on active metal species was demonstrated, taking into account the values shown in Fig. 8.

As a general tendency, a relationship between the capacity of the solids to produce AA and the average temperature of H_2 desorption ($T_{1/2}$), corresponding to the H_2 desorption in the first temperature interval (Fig. 2), occurred as can be seen in Fig. 8. Thus, the Co oxide species in the impregnated systems that were the easiest to reduce (lower $T_{1/2}$ values), exhibited a higher activity to produce acrylic acid, not only more than the phosphates containing Co, but also more than the rest of

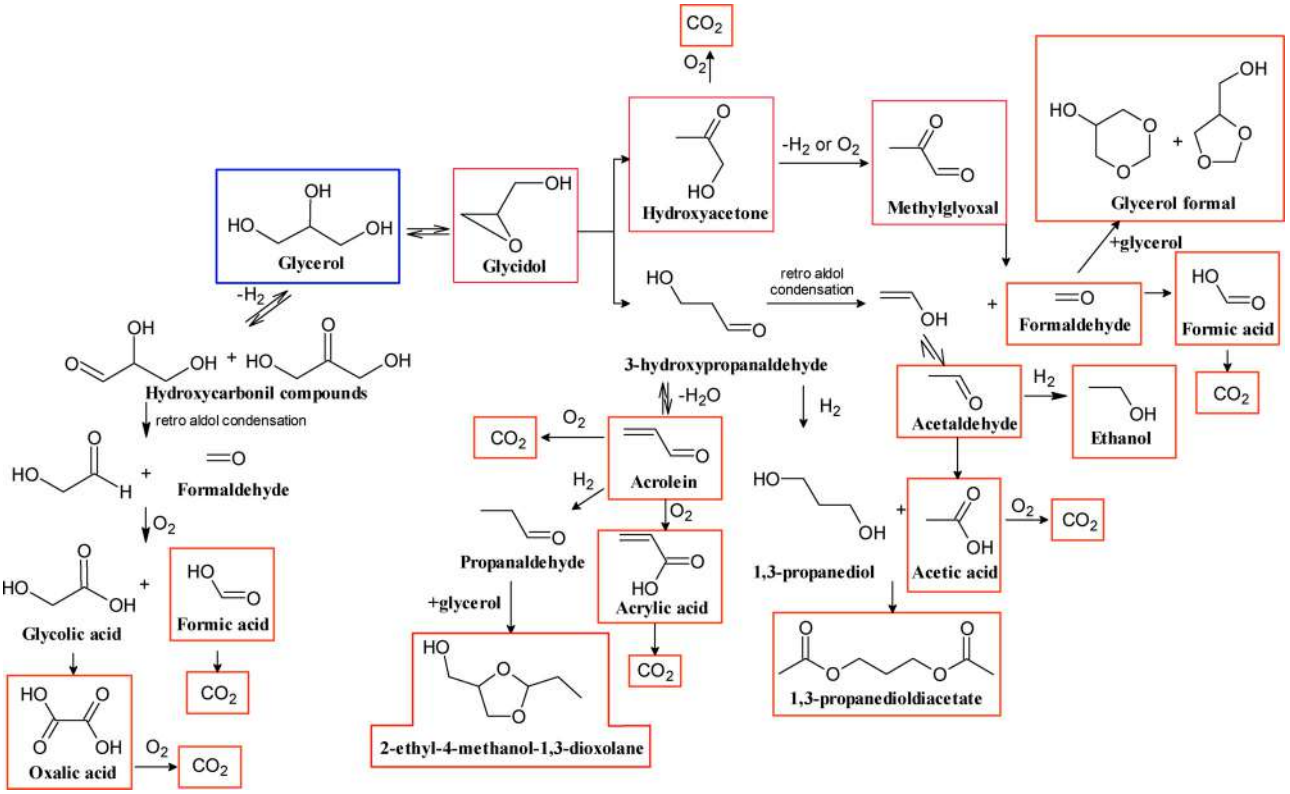

Scheme 1. Possible reactions involved in the glycerol transformation. The detected products are represented by rectangles.

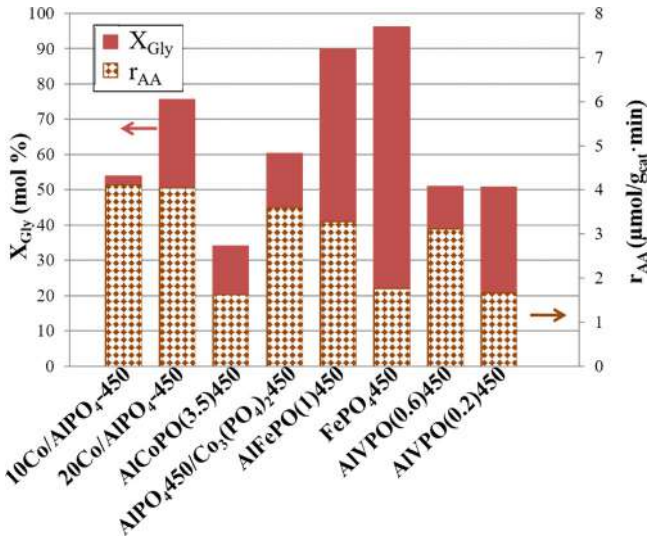

Fig. 7. Glycerol conversion (X_{Gly}) and rate of acrylic acid production (r_{AA}) values on all the solids studied. Reaction conditions: 36 wt% glycerol; F_{Gly} = 0.7 μmol/s; F_{N2} = 17 mL/min; F_{O2} = 2 mL/min; w = 0.2 g; 280 °C; time on stream = 3 h.

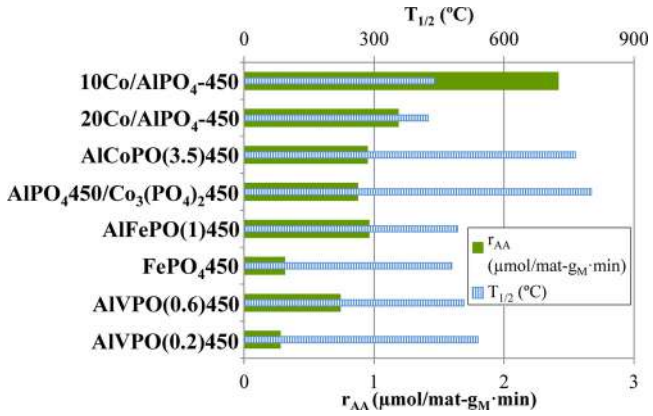

Fig. 8. Acrylic acid formation rate values, r_{AA} (μmol/mat-g_M·min), and of average temperature of H_2 desorption ($T_{1/2}$) obtained on all the solids studied.

the catalysts.

On all solids studied, other products in addition to acrylic acid were formed. In fact, as can be seen in Fig. 9 and in Table 4, the rate of formation of the majority of these products and the selectivity values, were appreciably higher than those of acrylic acid. In general, acrolein was the main product obtained in clear accordance with that reported in the literature [3,16,21,22]. As happened in the absence of oxygen [26,27] under the present experimental conditions, the solids with Fe were the most active in the acrolein formation, but also in the formation of acetic acid and CO_2, as well as in that of MG, although they hardly showed any activity in the hydroxyacetone formation. Contrarily, the systems with Co, showed a similar activity in the formation of both acrolein and hydroxyacetone, whereas the yields to CO_2 and MG were very low. The behaviour of the Al-V phosphates was intermediate as can be seen in Fig. 9 and Table 4. Furthermore, a higher percentage of V implied a higher yield to CO_2, as has been described [17–19].

There was no direct relation between the formation of highly oxidized compounds, including carbon dioxide, in the glycerol transformation and in the propene oxidation, Fig. 10. This result is probably because the propene oxidation does not proceed only via a Mars-van Krevelen mechanism, as aforementioned. Thus, the participation of molecular oxygen in its excited singlet state in the oxidation of propene cannot be ruled out, while the oxidation of acrolein to acrylic acid, or of other products in the glycerol transformation, should proceed by a Mars-van Krevelen mechanism. In this sense, it should be noted that $AlPO_4$ did not show activity in the formation of oxidized compounds in

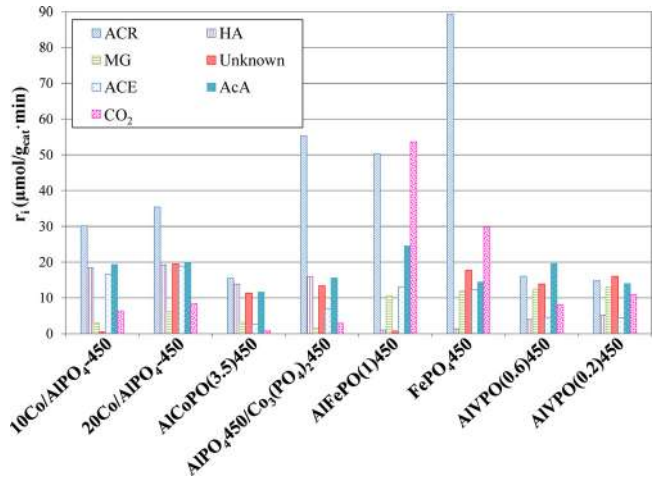

Fig. 9. Different products formation rate (r_i) on all the solids studied. (Experimental conditions as in Fig. 7).

Table 4
Values of selectivity to the main products obtained on all the solids studied. Reaction conditions: 36 wt% glycerol; F_{Gly} = 0.7 µmol/s; F_{N2} = 17 mL/min; F_{O2} = 2 mL/min; w = 0.2 g; 280 °C; time on stream = 3 h.

Catalyst	Selectivity (mol%)								
	ACRO	HA	MG	GF	Unknown	AA	ACE	AcA	CO_2
10Co/AlPO$_4$-450	27	16	3	6	1	4	15	17	6
20Co/AlPO$_4$-450	22	12	4	6	12	3	12	13	5
AlCoPO(3.5)450	22	19	4	7	16	2	4	16	1
AlPO$_4$450/ Co$_3$(PO$_4$)$_2$450	44	13	1	5	11	3	6	12	2
AlFePO(1)450	27	1	6	6	1	2	7	13	28
FePO$_4$450	44	1	6	5	9	1	6	7	15
AlVPO(0.6)450	15	4	12	11	13	3	4	18	8
AlVPO(0.2)450	14	5	12	10	15	2	4	13	10

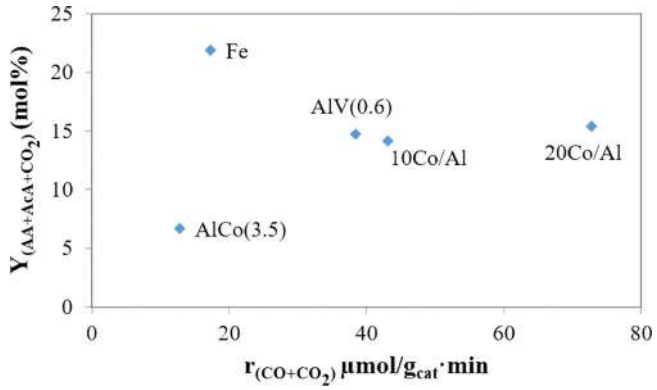

Fig. 10. Yield to oxidized compounds in the glycerol transformation versus the rate of carbon oxide formation in the oxidation of propene.

the glycerol transformation, therefore catalysts with redox sites being necessary. The activation of molecular oxygen could take place on Lewis acid sites of $AlPO_4$, as reported previously in the oxidative dehydrogenation of ethylbenzene [41], the reaction temperature being a key parameter. Thus, the temperature employed in the glycerol transformation, 280 °C, would not be high enough to activate the molecular oxygen, whereas that employed in the propene conversion, 400 °C, would be adequate. As shown in Fig. 10, the Al-Co binary phosphate promoted the total oxidation, as well as the formation of acrylic acid, to a lesser degree than the supported systems. A possible explanation for this result could be in the lower tendency to reduce (Fig. 2) and acid site

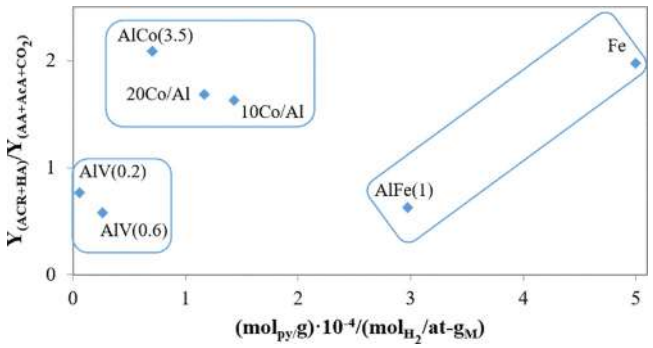

Fig. 11. Dehydration/oxidation compounds ratio in the glycerol transformation versus acidity/H_2 consumption.

density (Table 1) that this binary phosphate exhibited.

On the other hand, the ratio between the capacity to produce dehydration compounds (yield to acrolein and hydroxyacetone) and the capacity to produce oxidation compounds (yield to acrylic acid, acetic acid and CO_2) from glycerol is presented in Fig. 11, not affecting the differences in the superficial area values of the catalysts. The vanadium systems exhibited a higher capacity to produce oxidation compounds than dehydration compounds, whereas the systems containing Co presented an inverse behaviour. Among the Co systems, the binary phosphate provided less oxidation total products than the corresponding supported system, as aforementioned, though the phosphate exhibited a smaller ratio between acidity (Table 1) and H_2 consumption (Table 2) (Py/H_2) than the supported system. This result, which did not happen in the case of the solids containing iron, could be explained taking into account not only the number of redox sites, but also their tendency to be reduced that is lower in the redox sites existing in the Al-Co phosphate (Fig. 2 and Table 2). Moreover, the acid sites apart from enabling dehydration, would also contribute to the oxidation of the acrolein and/or other molecules retaining them, thus favouring its subsequent oxidation. Hence, a balance between redox and acid properties, in number and strength, seems to be the key to obtaining high yields to acrylic acid, avoiding the total oxidation to carbon oxides, according to Nieto et al. [24]. Based on the present results, among the metals investigated here, Co would form part of the required catalyst. In this sense, research is being developed in order to design an appropriate catalyst and to advance in the knowledge of the mechanism of formation of acrylic acid from glycerol.

4. Conclusions

At 280 °C and O_2/Gly = 2 molar ratio, the highest values of glycerol conversion (around 90%) were obtained for the solids containing Fe, followed by those with Co (around 75%), and finally by those with V (around 50%). However, the most active solids in the acrylic acid formation were the two Co supported systems, which exhibited a similar yield value (~2 mol%). Likewise, the presence of Al in the Fe and V phosphates promoted the formation of acrylic acid. In general, more activity in the acrylic acid formation also implied more activity in the formation of acetic acid and carbon dioxide. In fact, the rate of formation of these oxidized compounds was appreciably higher than that of acrylic acid on all solids studied, as also happened in the propene oxidation, where the formation of carbon oxides was noticeably superior to that of acrolein. Some possible reactions involved in the glycerol transformation into oxidized compounds, have been suggested.

In addition to the oxidized compounds, the formation of dehydration compounds (mainly acrolein and hydroxyacetone) from glycerol took place, the binary Al-V and Al-Fe phosphates showing a higher capacity to produce oxidation compounds than dehydration compounds, whereas the systems containing Co presented an inverse behaviour. This result could be related not only with the ratio between

number of acid and redox sites exhibited by the catalysts, but also with the facility to be reduced of the redox sites. Moreover, the acidity of the solids favoured the dehydration of glycerol to acrolein, but also the retention of this molecule or other ones, promoting their subsequent oxidation. Hence, a balance between redox and acid properties, in number and strength, seems to be the key to obtaining high yields to acrylic acid, avoiding the total oxidation to carbon oxides. Based on the present results, of the metals investigated here, Co would be the best candidate in the formulation of a hypothetical catalyst for the oxide-hydration of glycerol. In this sense, research is being developed in order to design an appropriate catalyst and to advance in the knowledge of the formation of the acrylic acid mechanism from glycerol.

Acknowledgements

Subsidies granted by the Ministerio de Economia, Industria y Competitividad (MINECO) and FEDER funds (Project ENE2016-81013-R) and Junta de Andalucía and FEDER funds (P11-TEP-7723) are gratefully acknowledged. S. Lopez-Pedrajas is indebted to the Ministerio de Educación, Ciencia y Deporte (MECD) for a FPU fellowship. The authors are thankful to the staff at the Central Service for Research Support (SCAI) of the University of Córdoba for their assistance.

References

[1] P.S. Kong, M.K. Aroua, W.M.A.W. Daud, Renew. Sust. Energ. Rev. 63 (2016) 533–555.
[2] X. Luo, X. Ge, S. Cui, Y. Li, Bioresour. Technol. 215 (2016) 144–154.
[3] A. Witsuthammakul, T. Sooknoi, Appl. Catal. A-Gen. 413 (2012) 109–116.
[4] Y.S. Yun, K.R. Lee, H. Park, T.Y. Kim, D. Yun, J.W. Han, J. Yi, ACS Catal. 5 (2014) 82–94.
[5] A. Drochner, D. Ohlig, S. Knoche, N. Gora, M. Heid, N. Menning, T. Petzold, H. Vogel, Top. Catal. 59 (2016) 1518–1532.
[6] K.Y. Koltunov, V.I. Sobolev, V.M. Bondareva, Catal. Today 279 (2017) 90–94.
[7] J. Liu, F. Mohamed, J. Sauer, J. Catal. 317 (2014) 75–82.
[8] S.A. Holmes, J. Al-Saeedi, V.V. Guliants, P. Boolchand, D. Georgiev, U. Hackler, E. Sobkow, Catal. Today 67 (2001) 403–409.
[9] G. Mestl, J.L. Margitfalvi, L. Végvári, G.P. Szijjártó, A. Tompos, Appl. Catal. A-Gen. 474 (2014) 3–9.
[10] M.E. Davis, Top. Catal. 58 (2015) 405–409.
[11] A. Galadima, O. Muraza, J. Taiwan, Inst. Chem. Eng. 67 (2016) 29–44.
[12] S. Thanasilp, J.W. Schwank, V. Meeyoo, S. Pengpanich, M. Hunsom, Chem. Eng. J. 275 (2015) 113–124.
[13] B. Sarkar, C. Pendem, L.S. Konathala, R. Tiwari, T. Sasaki, R. Bal, Chem. Commun. 50 (2014) 9707–9710.
[14] S. Thanasilp, J.W. Schwank, V. Meeyoo, S. Pengpanich, M. Hunsom, J. Mol, Catal. A-Chem. 380 (2013) 49–56.
[15] J. Deleplanque, J.-L. Dubois, J.-F. Devaux, W. Ueda, Catal. Today 157 (2010) 351–358.
[16] F. Wang, J. Xu, J.L. Dubois, W. Ueda, ChemSusChem 3 (2010) 1383–1389.
[17] M.D. Soriano, P. Concepción, J.M. Lopez Nieto, F. Cavani, S. Guidetti, C. Trevisanut, Green Chem. 13 (2011) 2954–2962.
[18] A. Chieregato, F. Basile, P. Concepción, S. Guidetti, G. Liosi, M.D. Soriano, C. Trevisanut, F. Cavani, J.M. Lopez Nieto, Catal. Today 197 (2012) 58–65.
[19] L. Shen, H. Yin, A. Wang, X. Lu, C. Zhang, Chem. Eng. J. 244 (2014) 168–177.
[20] A. Chieregato, M.D. Soriano, F. Basile, G. Liosi, S. Zamora, P. Concepción, F. Cavani, J.M. Lopez Nieto, Appl. Catal. B-Environ. 150–151 (2014) 37–46.
[21] R. Liu, T. Wang, D. Cai, Y. Jin, Ind. Eng. Chem. Res. 53 (2014) 8667–8674.
[22] L.G. Possato, W.H. Cassinelli, T. Garetto, S.H. Pulcinelli, C.V. Santilli, L. Martins, Appl. Catal. A-Gen. 492 (2015) 243–251.
[23] L. Liu, B. Wang, Y. Du, Z. Zhong, A. Borgna, Appl. Catal. B-Environ. 174–175 (2015) 1–12.
[24] A. Chieregato, C. Bandinelli, P. Concepción, M.D. Soriano, F. Puzzo, F. Basile, F. Cavani, J.M. Lopez Nieto, ChemSusChem 9 (2016) 1–12.
[25] R. Estevez, S. Lopez-Pedrajas, F. Blanco-Bonilla, D. Luna, F.M. Bautista, Chem. Eng. J. 282 (2015) 179–186.
[26] S. Lopez-Pedrajas, R. Estevez, R. Navarro, D. Luna, F.M. Bautista, J. Mol, Catal. A-Chem. 421 (2016) 92–101.
[27] S. Lopez-Pedrajas, R. Estevez, F. Blanco-Bonilla, D. Luna, F.M. Bautista, J. Chem, Technol. Biotechnol. 92 (2017) 2661–2672.
[28] R. Navarro, S. Lopez-Pedrajas, D. Luna, J.M. Marinas, F.M. Bautista, Appl. Catal. A-Gen. 474 (2014) 272–279.
[29] F.M. Bautista, J.M. Campelo, A. García, D. Luna, J.M. Marinas, A.A. Romero, M.T. Siles, Catal. Today 78 (2003) 269–280.
[30] F.M. Bautista, B. Delmon, Appl. Catal. A-Gen. 130 (1995) 47–65.
[31] F.M. Bautista, J.M. Campelo, A. Garcıa, D. Luna, J.M. Marinas, R.A. Quiros, A.A. Romero, Appl. Catal. A-Gen. 243 (2003) 93–107.
[32] M.H. Woo, J.M. Cho, K.W. Jun, Y.J. Lee, J.W. Bae, ChemCatChem 7 (2015) 1460–1469.
[33] J.W. Bae, S.-M. Kim, S.-H. Kang, K.V. Chary, Y.-J. Lee, H.-J. Kim, K.-W. Jun, J. Mol, Catal. A-Chem. 311 (2009) 7–16.
[34] L. Wang, D. Li, H. Watanabe, M. Tamura, Y. Nakagawa, K. Tomishige, Appl. Catal. B-Environ. 150 (2014) 82–92.
[35] P. Nagaraju, N. Lingaiah, M. Balaraju, P.S. Sai Prasad, Appl. Catal. A-Gen. 339 (2008) 99–107.
[36] N. Pasupulety, H. Driss, Y.A. Alhamed, A.A. Alzahrani, M.A. Daous, L. Petrov, N. Lingaiah, P.S. Prasad, J. Chem. Sci. 128 (2016) 227–234.
[37] E. Hensen, Q. Zhu, P.-H. Liu, K.-J. Chao, R. van Santen, J. Catal. 226 (2004) 466–470.
[38] F.M. Bautista, J.M. Campelo, D. Luna, J. Luque, J.M. Marinas, M.T. Siles, Chem. Eng. J. 120 (2006) 3–9.
[39] F. Blanco-Bonilla, S. Lopez-Pedrajas, D. Luna, J.M. Marinas, F.M. Bautista, J. Mol, Catal. A-Chem. 416 (2016) 105–116.
[40] C. Zhao, I.E. Wachs, J. Phys. Chem. C 112 (2008) 11363–11372.
[41] F.M. Bautista, J.M. Campelo, A. Garcia, D. Luna, J.M. Marinas, J. Catal. 116 (1989) 338–349.